Light-harvesting in mesophotic corals is powered by a spatially efficient photosymbiotic system between coral host and microalgae

Netanel Kramer[1*], Raz Tamir[1,2], Or Ben-Zvi[1,2], Steven L. Jacques[3], Yossi Loya[1], Daniel Wangpraseurt[4,5]

[1] *School of Zoology, Tel-Aviv University, Tel Aviv 69978, Israel*

[2] *The Interuniversity Institute for Marine Sciences of Eilat, Eilat 88103, Israel*

[3] University of Washington, Seattle, USA

[4] *Department of Nanoengineering, University of California San Diego, San Diego, USA*

[5] *Department of Chemistry, University of Cambridge, Cambridge, UK*

Corresponding author: Netanel Kramer <nati.kramer@gmail.com>

Summary

The coral-algal photosymbiosis fuels global coral-reef primary productivity, extending from sea level to as deep as 150 m (i.e., mesophotic). Currently, it is largely unknown how such mesophotic reefs thrive despite extremely limited light conditions. Here, we show that corals exhibit a plastic response to mesophotic conditions that involves a spatially optimized regulation of the bio-optical properties by coral host and symbiont. In contrast to shallow corals, mesophotic corals absorbed up to three-fold more light, resulting in excellent photosynthetic response under light conditions of only ~3% of the incident surface irradiance. The enhanced light harvesting capacity of mesophotic corals is regulated by average refractive index fluctuations in the coral skeleton that give rise to optical scattering and facilitate light transport and absorption by densely pigmented host tissue. The results of this study provide fundamental insight into the energy efficiency and light-harvesting mechanisms underlying the productivity of mesophotic coral reef ecosystems, yet also raise concerns regarding their ability to withstand prolonged environmental disturbances.

Keywords: *Light-harvesting*; *Bio-optics*; *Photobiology*; *Ecophysiology*; *Mesophotic Coral Ecosystems (MCEs)*; *Red Sea*

Introduction

Scleractinian corals are the primary building blocks of coral reef ecosystems. Coral calcification involves the secretion of aragonite skeleton that provides the basis of the three-dimensional topography and complexity of coral reefs [1]. The underlying success of corals as ecosystem engineers is mainly due to the complex interaction that takes place between the coral hosts and their endosymbiont microalgae (family: Symbiodiniaceae). The coral-algal symbiosis is driven by solar energy and acts as the biological engine fueling the reef [2]. Corals have adapted to capture and maximize light under various environmental conditions, and it has been suggested that they are among the most efficient photosynthetic organisms at utilizing and converting light energy [3–6].

However, the symbiotic interaction is susceptible to anthropogenically mediated changes in environmental conditions [7]. Specifically, the coral-algal symbiosis is affected by periods of prolonged thermal stress, which can lead to a breakdown of the symbiosis and the visible paling of corals, known as coral bleaching [8]. Coral bleaching events have increased in frequency and duration over the last few decades, leading to an unprecedented decline of coral reefs worldwide [9]. The combined effects of elevated ocean temperatures, ocean acidification, and intensifying storms, have resulted in a decline in coral growth and functioning, due to reduced fecundity [10] and recruitment stock [11], reproductive synchronization breakdown [12], and coral disease outbreaks [13], thereby impairing the persistence of corals through environmental disturbances [14–16].

Most efforts to promote the recolonization of degrading shallow coral reefs have been focused on shallow-water corals [17]. More recently, it has been considered that mesophotic coral ecosystems (MCEs; > 30 m) are potential sources of replenishment and sinks for avoiding disturbances, since they could offer protection from the harmful environmental impacts encountered by their shallow-reef counterparts [18–20]. However, it has been shown that deep-

water reefs can experience impacts from extreme storms and heatwaves, although not at the same frequency or intensity as in the shallow environments [21–23].

Coral morphological plasticity in response to environmental changes, is thought to enable corals to inhabit a wider range of environments and increase their ability to withstand disturbances [24–26]. Coral species that are distributed throughout a wide depth range (known as "depth-generalists") adjust certain life-history traits in response to differences in irradiance [27]. It was found that light quantity affects coral morphology and growth rates [28,29], community composition [30,31], recruitment patterns [32–34], reproduction [35], and photobiology [27]. For instance, faster-growing species are found in well-lit shallow waters, while in deeper waters, decreasing levels of photosynthetically active radiation (PAR, 400-700 nm) typically result in reduced linear extension and coral calcification rates [28].

Although irradiance is fundamental for coral photosynthesis, excess light can easily result in photodamage to the photosynthetic apparatus [2]. Corals, therefore, employ a range of mechanisms to adjust light-harvesting and photosynthesis in response to the ambient light environment, most commonly by regulating their morphological structure [36,37], chlorophyll-*a* concentrations and/or cell densities [38,39]. Light-harvesting efficiency in corals is strongly controlled by the light scattering and absorption properties of coral host and symbionts. The light-scattering properties of coral host tissue and the aragonite skeleton play a key role in modulating the *in-hospite* light environment that controls photosynthesis [3,4]. While earlier coral optics studies have focused on the apparent optical properties (i.e. light field parameters), recent advances in experimental techniques enable the study of inherent optical properties (e.g., absorption and scattering coefficients) which depend on the material properties and structure of corals and are independent of illumination conditions [40–42]. For some corals, it has been shown that the high scattering of the living tissue traps light, while the low absorption and

91 scattering of the skeleton redistribute the light that penetrates the living tissue, enabling the
92 light to reach otherwise shaded living tissue [41].

93 The broad array of morphological forms found in corals indicates potentially important
94 consequences in regard to regulation of the optical properties of the individual coral species
95 [5,29,36]. In MCEs, corals can be found thriving at the PAR limits (0.1-1% of surface
96 irradiance; see Tamir *et al.* 2019), which suggests that they have developed strategies to cope
97 with and adjust to such extreme light habitats. Compared to shallow-water corals, those
98 inhabiting mesophotic reefs exhibit unique characteristics that optimize photosynthetic
99 efficiency [43–45]. Corals maximize their surface area at the morphological level to primarily
100 laminar, plate-like morphologies allowing for a maximized light capture [43,46]. Furthermore,
101 it has been suggested that fluorescent proteins can also promote the adaptation to low-light
102 environments, by converting blue light into orange-red light, which can penetrate deeper within
103 the coral tissues [43,47]. However, due to the previous inaccessibility of MCEs, our
104 understanding of the bio-optical properties and ecophysiology of mesophotic corals are
105 preliminary.

106 Here, we studied the ecophysiology and bio-optical properties of four widely depth-
107 distributed coral species from shallow (5-10 m) and mesophotic (40-45 m) depths in the Gulf
108 of Eilat/Aqaba, Red Sea. We aimed to elucidate the bio-optical mechanisms that enable corals
109 to adapt to low-light environments, and hypothesized that corals in mesophotic environments
110 would display bio-optical properties optimized to absorb low-light. Specifically, we employed
111 a combination of techniques to study the photophysiology, *in-vivo* light field parameters, and
112 the inherent optical properties of corals. The results of this study present an explanation of the
113 processes that drive the photobiology and ecophysiology of mesophotic corals and shed light
114 on how mesophotic corals may respond to environmental stress.
115

Results

Biometric assays

Algal pigmentation and density varied among species and within depths, with mesophotic specimens exhibiting an increase in pigmentation, as visible in the darker colored tissues (Fig. 1). Algal symbiont density (cells cm^{-2}) was on average three-fold higher in the mesophotic corals than in their shallow counterparts (MEPA, $p < 0.001$; Fig. 2a), with the highest cell count measured in the mesophotic *P. lobata* at $6.57\times10^5 \pm 1.11\times10^5$ cells per cm^2. Likewise, chlorophyll-*a* content (µg cm^{-2}) was enhanced in mesophotic vs. shallow specimen (0.41-2.75 vs 0.014-0.94 µg cm^{-2}, respectively; MEPA, $p < 0.01$; Fig. 2b). Overall, chlorophyll-*a* content per cell (pg $cell^{-1}$) was higher in mesophotic corals (MEPA, $p < 0.05$; Fig. 2c), except for *S. pistillata* which exhibited similar concentrations between depths (*Hg* = -0.03 [$CI_{95\%}$ -0.99; 0.99]).

Photosynthetic parameters

The maximum quantum yield of PSII (F_v/F_m) was significantly higher for mesophotic species (MEPA, $p < 0.05$) compared to their shallow-water counterparts (F_v/F_m = 0.50-0.72 and 0.19-0.65, respectively; $p < 0.05$), with shallow *P. lobata* exhibiting 50% lower F_v/F_m values compared to all other shallow-water specimens (Fig. 2d). Areal net photosynthesis (µmol O_2 cm^{-2} h^{-1}) differed between branching species, as well as between depths within species (MEPA, $p < 0.05$). On average, the light-use efficiency (α) of areal net photosynthesis was three-fold higher for mesophotic corals compared to shallow-water corals (MEPA, $p < 0.05$; Fig. 3a, e). *S. pistillata* corals displayed the largest differences in α between depths, with values nine-fold higher in the mesophotic specimen than in their shallow-water counterparts ($6.43\times10^{-2} \pm 3.33\times10^{-2}$ vs $7.43\times10^{-3} \pm 1.66\times10^{-3}$, respectively, Fig. 3a). Areal P_{MAX} was enhanced for mesophotic corals compared to shallow ones, as can be seen for example in the

two-fold higher P_{MAX} in mesophotic *A. squarrosa* corals (*Hg* = 1.63 [$CI_{95\%}$ 0.774; 3.18]). Moreover, P_{MAX} for mesophotic corals was achieved at almost one order of magnitude greater than in their ambient light environment (i.e., ~300 vs ~45 µmol photons m^{-2} s^{-1}, Fig. 1i). All mesophotic specimens displayed significantly lower E_K values than their shallower counterparts (MEPA, $p < 0.01$). In contrast to areal photosynthesis, cell-specific maximal rates in shallow *S. pistillata* exceeded those of their mesophotic counterparts by 30% (Table S1). The normalization for cell density also led to similar P_{MAX} values between shallow and mesophotic *A. squarrosa* (*Hg* = 0.66 [$CI_{95\%}$ -0.66; 1.82]). The normalization of O_2 production per unit cellular chlorophyll-*a* (µmol O_2 pg chl-a^{-1} s^{-1}) resulted in over two-fold greater α values for mesophotic corals (Table S1) and approximately 35% higher P_{MAX} for shallow corals (MEPA, $p < 0.05$; Fig. 3c,g).

P vs E_d was corrected for the *in vivo* photon scalar irradiance (E_0; PAR integrated over 400-700 nm) for all the photosynthetic parameters. This correction resulted in an over 50% increase in E_K values (E_d; Table S1). For example, in shallow *A. squarrosa* corals, light saturation levels of *P* vs E_0 reached ~180% of the *P* vs E_d (368.43 ± 79.40 and 206.73 ± 43.47 µmol photons m^{-2} s^{-1}, respectively), whereas, in mesophotic corals, E_K reached ~140% of the incident downwelling irradiance (91.85 ± 5.04 and 65.19 ± 3.03 µmol photons m^{-2} s^{-1}, respectively; Fig. 3). There was no significant trend in dark respiration between all species and depths (Table S2; Fig. 3a, e). For massive coral species, no clear differences were found in photosynthetic parameters (Table S1).

Bio-optical properties

Scalar irradiance (E_0) at the coral tissue surface differed among species and depths for both tissue areas (i.e., coenosarc and polyp). Shallow corals exhibited 22% and 33% higher E_0 at 675 nm than mesophotic corals for coenosarc and polyp areas, respectively (MEPA, $p <$

166 0.001; Fig. 4a-d). Scalar irradiance was consistently higher over the coenosarc tissue than over
167 the polyp tissue in both shallow and mesophotic *S. pistillata* corals (Fig. 4d), whereas E_0
168 differences between these areas in *P. lobata* varied only between depths, i.e., coenosarc was
169 higher in shallow corals and lower in their mesophotic counterparts (Fig. 4c). Attenuation of
170 PAR from tissue surface towards the skeleton was greater in mesophotic corals and was most
171 pronounced in *P. peresi*, with E_0 reaching down to 24% of E_d (Fig. S1). E_0 at the tissue-skeleton
172 interface was approximately two-fold higher for shallow corals compared to mesophotic corals
173 (MEPA, $p < 0.001$), ranging from 49.00 ± 0.88% to 158 ± 4.15% (mean ± SE; at 675 nm) of
174 the incident downwelling irradiance. Intra-tissue measurements were not performed in *P.*
175 *lobata* due to their extremely thin tissue.

176 Skeleton scalar irradiance over corallite (polyp skeleton) areas of shallow and
177 mesophotic corals were higher than over the coenosarc (MEPA, $p < 0.001$). For example,
178 shallow *S. pistillata* corals exhibited nearly 50% higher skeleton scalar irradiance over corallite
179 than over coenosarc, contrasting the pattern observed for intact corals (Fig. 4d). Compared to
180 mesophotic corals, both the shallow massive coral species exhibited significantly 15% lower
181 scalar irradiance over coenosarc (*P. peresi*: $Hg = 1.95$ [$CI_{95\%}$ 1.56; 2.34]; *P. lobata*: $Hg = 1.81$
182 [$CI_{95\%}$ 1.6; 2.04]), while no significant differences were found in the branching corals between
183 depths.

184 The spectral diffuse reflectance (%) of corals varied among species, depths, and
185 between live (tissue) and skeleton surfaces (MEPA, $p < 0.001$; Fig 4e-f). Tissue reflectance
186 was systematically higher for shallow corals and ranged between 14.80 ± 0.26% to 25.20 ±
187 0.36% compared to 6.36 ± 0.10% to 14.70 ± 0.40% for their mesophotic counterparts (in λ =
188 675nm; Fig. 4e, f). Excluding *A. squarrosa*, coral skeletons from the mesophotic reflected up
189 to 57% more light than their shallow counterparts ($Hg = -1.71$ [$CI_{95\%}$ -1.91; -1.52]; Fig. 4e).

The extracted algal absorption coefficient (μ_{a_algae}; cm^{-1}) for the four coral species ranged between 0.09 to 1.18 cm^{-1} at 675 nm (Fig. 5a-d, S2; Table 1). A comparison of shallow and mesophotic μ_{a_algae} revealed that for most mesophotic specimens μ_{a_algae} was at least two-fold greater. The largest difference was found for *A. squarrosa* with an approximate eight-fold enhancement in μ_{a_algae} for mesophotic versus shallow corals. Skeletal optical parameters were extracted from the radial attenuation of the fluence rate at 720 nm (Fig. S3). Skeletal absorption was approximately two-fold higher in shallow versus mesophotic branching corals and was highest in the shallow *P. lobata* displaying 0.51 cm^{-1} (Fig. S4). The skeletal reduced scattering coefficient at 720 nm was relatively similar between shallow and mesophotic *S. pistillata* (15.12 and 13.5 cm^{-1}, respectively). In contrast, shallow *A. squarrosa*, *P. peresi*, and *P. lobata* demonstrated over two-fold higher μ_s' compared to the mesophotic corals. Monte Carlo simulations used the extracted IOPs to calculate tissue absorption and showed that mesophotic *A. squarrosa* and *P. lobata* corals absorbed over 80% of the flux in the tissue compared to 25-30% in the respective shallow corals. In contrast, this depth-dependent difference in flux absorption was less pronounced for *S. pistillata* and absorption was only about 15% greater in mesophotic corals (Table 1).

Discussion

Understanding the ability of corals to grow and thrive under extreme low light is a key question in the study of mesophotic coral ecosystems [48]. In line with our hypothesis, the findings indicate that mesophotic corals have bio-optical properties optimized to absorb low-light. Our findings revealed up to three-fold enhanced light absorption by mesophotic corals (Fig. 5, Table 1) and an outstanding photosynthetic response under a range of light conditions (Fig. 3).

We found that for all mesophotic corals, except for *A. squarrosa*, PAR reflectance from coral skeletons was enhanced by up to 30% higher compared to shallow corals (Fig. 4). This shows that greater skeletal reflectance enhances light-harvesting by its photosymbionts [3], as exhibited by most mesophotic corals compared to their shallow counterparts (Fig. 4). We also detected a strong upregulation of light-absorbing pigments in all mesophotic coral tissues, due to both a higher algal cell density and enhanced chlorophyll-*a* per cell (Fig. 2), resulting in up to one order of magnitude higher algal absorption coefficients for mesophotic versus shallow-water corals (Fig. 5, Table 1). Such marked differences in algal absorption coefficient have not been previously characterized and indicate the presence of highly adapted light-harvesting complexes to low-light conditions. This is supported by earlier studies on mesophotic photobiology, demonstrating both an increase in the effective antenna size (i.e., antenna pigments) per photosynthetic unit (PSU) and an increase of PSUs per cell [44,49].

Although the upregulation of photosynthetic pigments can naturally give rise to algal self-shading [3], microscopic light sensor measurements inside the tissue of mesophotic corals revealed that the light available at the tissue-skeleton interface is surprisingly high, leaving approximately one-fourth of the incident light after photon absorption (Fig. S1). It is possible, therefore, that the enhanced skeletal reflectance acts as an effective strategy counterbalancing the effects of self-shading, by upregulating the diffuse light available from the skeleton to compensate for higher cell densities.

We further found spatial differences in the microscale distribution of light between intact corals and bare skeletons (Fig. 4). For *S. pistillata* corals, tissue scalar irradiance was up to 20% lower for polyp than for coenosarc tissue, similar to previous measurements in other coral species characterized by small polyps [4]. The reduced light intensity for polyp tissues matches the spatial distribution of endosymbionts with higher cell densities in polyp tissues than in coenosarc tissues (see Fig. 1a,e). Interestingly, the irradiance distribution for the bare

skeleton surface showed opposite patterns, indicating enhanced skeletal scattering within the polyp corallite than over the coenosarc. Therefore, enhanced light scattering within the corallite effectively assists in light dissipation to the dense microalgae inside the tissue. The high content of light-absorbing pigments within the polyp tissue (Fig. 4) suggests an increased biological activity of the coral polyp, and thus would require more light to support photosynthesis. Light availability within the corallite was strongly enhanced (Fig. 1S) which can be explained by intense scattering from the corallite skeletal walls toward its center [50], with additional light being transported to the polyp through the coenosteum [41]. Thus, the spatial distribution of the coral skeleton scattering and symbiont densities further support our hypothesis of a coral controlled finely tuned system of light scattering and light absorption.

Generally, both mesophotic *A. squarrosa* and *S. pistillata* corals utilized light more efficiently than their shallow counterparts, as indicated by steeper initial slopes of the *P-E* curves (Fig. 3a,d). For example, in *A. squarrosa* corals, the predicted net photosynthesis at a typical mid-day irradiance of 40-50 μmol photons m^{-2} s^{-1} in 45 m (Fig. 1i) was shown to be six-fold higher in mesophotic versus shallow depths (Fig. 3a). Still, we found species-specific differences in photosynthetic rates. Upon normalizing P_n to algal cell density, *S. pistillata* revealed a typical light-shade response between depths (Fig. 3e), i.e., lower P_{MAX} and E_K values for mesophotic individuals [39,49]. In contrast, *A. squarrosa* did not follow this pattern and mesophotic corals exhibited higher P_{MAX} and E_K values when photosynthetic rates were normalized to cell density (Fig. 3b). However, when *P-E* curves were calculated based on chlorophyll-*a* content, *A. squarrosa* displayed a typical light-shade response, similar to *S. pistillata* (Fig. 3c,f).

The extraction of the inherent optical properties of corals allowed for a novel development of a probability distribution model that predicts the total flux absorbed within the photosynthetic coral tissue of shallow and mesophotic corals (Fig. 5, Table 1). The combination

of increased reflectivity, high algal absorption coefficient, and low μ_s' (i.e., higher lateral spread of light) facilitated a strikingly higher total absorbed flux by mesophotic corals as compared with shallow ones. The mesophotic *A. squarrosa* and *P. lobata* showed approximately three-fold higher flux absorption than the shallower counterparts, whereas for *S. pistillata* there was only a ~20% difference between shallow and mesophotic specimen (Table 1). These findings indicate that in contrast to *A. squarrosa*, *S. pistillata* corals show light-regulated host modifications, as also supported by the pronounced differences in scalar irradiance between corallite and coenosarc areas, as well as between depths (Fig. 4d). Moreover, minor skeletal scattering differences between depths may be explained by micro-architectural modifications that compensate for changes in the skeletal material properties at mesophotic depths, as recently reported for this species [55]. This supports the notion that the ability of *S. pistillata* to adapt to different light regimes is not limited by its photosymbionts [53].

It is important to note that the energetic demands required to sustain coral growth at low-light can be further achieved through supplementation derived from heterotrophy (e.g., predation of zooplankton) [52]. However, since heterotrophic feeding is thought to be species-specific, the strategy of increased reliance on heterotrophy versus autotrophy with depth does not appear to be a primary trophic strategy for some depth-generalists, and particularly not in deep-water specialists [45]. The photosynthetic and growth efficiencies of the strictly mesophotic *Leptoseris* species, for example, were shown to be facilitated mainly by their skeletal optical geometry [45].

The advantage of low-light optimized bio-optical properties in mesophotic corals may prove to be their weakness in times of thermal stress. Although considered a relatively stable environment, MCEs can experience extreme heat-waves that lead to coral bleaching [22]. During bleaching in shallow corals, it has been shown that endosymbiotic algae are exposed to

289 enhanced irradiance from skeletal backscattering, which can further stimulate symbiont loss, a
290 hypothesis referred to as the "optical-feedback loop" [42,50]. Different factors have been
291 shown to be related to enhanced bleaching susceptibility, such as lower μ_s' [42,54], enhanced
292 skeletal reflectivity [50], and high photosymbiont densities [56], all of which have been
293 demonstrated here by the mesophotic specimen (Fig. 3,5,6). Hence, the combination of these
294 factors suggests that mesophotic corals are more susceptible to bleaching than their shallower
295 counterparts. In an era of rapid climate change, it is therefore critical to assess the effects of
296 thermal stress on mesophotic corals.

297 Thermal stress, however, is only one of many contemporary threats that coral reefs must
298 face in a changing climate. Ocean acidification, in particular, was shown to impair the capacity
299 of corals to build their skeletons through calcification [57,58]. An effective dissipation of light
300 from the coral relies on a proper balance between the skeletal scattering and absorption,
301 however, increased porosity and skeletal deformation caused by ocean acidification [59] are
302 likely to disturb this balance. The light-harvesting process achieved by skeletal light scattering
303 may become compromised as a result, leading to far-reaching ecological consequences caused
304 by the coral's inability to regulate light and impaired mechanical integrity. Given that corals
305 are the main bioengineers in coral reefs, a reduction in coral growth will diminish the
306 structurally complex habitat needed for numerous species [60]. Unfortunately, in times of
307 change, this negative effect may be more pronounced in MCEs, since mesophotic corals could
308 be more vulnerable and express limited and/or slower adaptability [22]. Notwithstanding the
309 importance of corals as bioengineers, research focusing on the effects of altered environmental
310 parameters on the bio-optical properties of corals has not received sufficient study to date, and
311 more research is needed to determine the impact of projected near-future acidification levels,
312 coupled with other significant environmental factors.

313 In conclusion, we present bio-optical mechanisms employed to sustain coral growth in
314 extreme low-light environments, and expand the current knowledge on mesophotic
315 photobiology. Light-harvesting in mesophotic corals is facilitated by the combination of
316 pigment upregulation and enhanced skeletal reflectance. The light-harvesting strategies
317 employed by mesophotic corals enhanced the absorbed flux by up to three-fold compared to
318 their shallow counterparts, suggesting a spatially efficient photosymbiotic system. The results
319 of this study further suggest that such light harvesting strategies make mesophotic corals
320 specifically susceptible to environmental change and highlight the importance of integrating
321 bio-optics and ecology to predict the future response of coral reef ecosystems to climate
322 change.
323
324 **Author contributions**
325 N.K., Y.L., and D.W. conceived and designed the study; N.K., R.T., and D.W. collected the
326 corals; N.K., R.T., O.B.Z, and D.W. performed research; N.K., S.L.J, and D.W. analyzed the
327 data; N.K. wrote the manuscript with contributions and final approval from all authors.
328
329 **Acknowledgments**
330 We thank the Interuniversity Institute for Marine Sciences in Eilat (IUI) for making their
331 facilities available, and their staff for excellent assistance. O. Levy, D. de Beer, and T. Treibitz
332 are thanked for lending equipment. This work was supported by the Israel Science Foundation
333 (ISF) Grant No. 1191/16 to Y.L., the European Union's Horizon research and innovation
334 program under grant agreement No. 730984, and by the ASSEMBLE-Plus consortium grant to
335 D.W.
336
337

Figure Legends

Figure 1. Morphotypes of depth-generalist corals and PAR profile. Studies species from shallow (5-10 m; **a-d**) and mesophotic (40-45 m; **e-h**) depths, at colony level and polyp-coenosarc level (insets; scale bars = 0.5 and 1 mm in branching and massive corals, respectively). Insets were taken using the same optical microscope settings. (**i**) Mid-day photosynthetic active radiation (PAR; µmol photon m^{-2} s^{-1}) as a function of depth (m) in February, measured off the interuniversity institute for marine sciences in Eilat. Shallow (5-10 m; *light-blue*) and mesophotic (40-45 m; *dark-blue*) are shown as horizontal dotted lines, with a corresponding range of PAR values (*red*).

Figure 2. Biometric assays. Microalgal symbiont density (**a**), chlorophyll-*a* density (**b**), cellular chlorophyll-*a* (**c**), and F_v/F_m (**d**) for four depth-generalist coral species from shallow water (5-10 m; *light-blue*) and mesophotic water depths (40-45 m; *dark-blue*). Box plots depict the median (horizontal line), interquartile range (first and third quartiles), and whiskers as ±1.5 interquartile range with dots representing outliers (n = 9-27 repetitions per species per depth).

Figure 3. O_2 production for *A. squarrosa* (a-c) and *S. pistillata* (e-g) from shallow (5-10 m; *light-blue*) and mesophotic (40-45 m; *dark-blue*) depths. O_2 production is shown as areal net photosynthesis (µmol O_2 cm^{-2} h^{-1}; **a, e**), with gray dashed line represents 0 net photosynthesis; gross photosynthesis per algal cell (µmol O_2 $cell^{-1}$ h^{-1}; **b, f**); and gross photosynthesis per chlorophyll content (µmol O_2 pg chl-a^{-1} h^{-1}; **c, g**). Each photosynthetic measurement (P) was performed as a function of the downwelling photon irradiance (E_d; solid lines and filled circles) and of scalar photon irradiance (E_0; dashed lines and hollow circles) spanning eight irradiance levels. Curves were fit using a double exponential decay model [61]. Data points represent mean ± standard error (n = 9 repetitions per species per depth). Note that the x,y scales for *A. squarrosa* and *S. pistillata* have been adjusted for clarity.

Figure 4. Apparent optical properties at 400-700 nm. Coral scalar photon irradiance (E_0; % incident irradiance) at the tissue and skeleton surfaces, measured over the coenosarc (solid lines) and the polyp/corallite (dashed lines) areas (**a-d**). Normalized spectral reflectance of light ($R_d(\lambda)$; %) over the coral tissue and skeleton surfaces (**e-h**). Tissue surfaces are colored in blue shades (*light-blue* and *dark-blue* for shallow and mesophotic corals, respectively), and skeleton surfaces are colored in warm shades (*orange* and *dark-red* for shallow and mesophotic corals, respectively). Data are mean (thick lines) ± standard error (thin lines); n = 15-45 repetitions per species per depth.

374 **Figure 5. Inherent optical properties.** Algal absorption coefficient μ_{a_algae} (cm^{-1}) of isolated
375 microalgae at 675 nm as a function of microalgae density for shallow (*light-blue*) and
376 mesophotic (*dark-blue*) samples (**a-d**). Coral skeletal scattering (μ_s') and absorption coefficient
377 (μ_a) between 500-750 nm (data points) plotted against measured R_d for shallow and mesophotic
378 (hollow and filled circles, respectively; colors denote species) (**e**).
379

380 # Tables

381 **Table 1.** Inherent optical properties extracted from intact live corals (live at 675 nm) and bare
382 skeletons (at 720 nm) using diffusion theory: tissue and skeletal absorption coefficient (μ_a[cm^{-1}]), and skeletal scattering coefficient (μ_s' [cm^{-1}]). The predicted absorbed flux (watt per cm^{-2}
384 per watt delivered) of the tissue affected by the optical parameters was derived from Monte
385 Carlo simulations.

Species	**Depth**	**μ_a (tissue)**	**μ_a (skeleton)**	**μ_s' (skeleton)**	**Absorbed flux**
A. squarrosa	Shallow	0.09	0.40	36.00	0.25
	Mesophotic	0.81	0.22	12.84	0.82
P. lobata	Shallow	0.17	0.51	35.66	0.30
	Mesophotic	0.87	0.08	15.57	0.87
S. pistillata	Shallow	0.66	0.47	15.12	0.75
	Mesophotic	1.18	0.27	13.50	0.89

386
387
388
389
390
391
392

STAR METHODS

RESOURCE AVAILABILITY

Lead Contact

Requests for further information and data should be directed to and will be fulfilled by the lead contact, Netanel Kramer (nati.kramer@gmail.com)

Materials Availability

This study did not generate new unique materials.

Data and Code Availability

All datasets generated and/or analyzed during the study are available from the lead contact upon request.

EXPERIMENTAL MODEL AND SUBJECT DETAILS

Coral collection and maintenance

Mature intact colonies of four depth-generalist coral species were chosen for a comparative study between shallow and mesophotic water specimens. We selected two branching coral species (*Stylophora pistillata* and *Acropora squarrosa*), and two massive coral species (*Paramontastrea peresi* and *Porites lobata*) based on their contrasting skeletal morphologies and their occurrence across a large depth gradient [29,30]. Coral colonies (n = 3 per species per depth) were collected using recreational and technical diving at shallow (5-10 m) and mesophotic (40-45 m) depths, respectively, from the Gulf of Eilat/Aqaba, the Red Sea. Conspecific colonies were collected at least five meters apart to avoid sampling clonemates. Colonies were maintained in outdoor open-circuit seawater tables at the Interuniversity Institute (IUI) in Eilat. Mesophotic colonies were kept in separate seawater tables under a blue

light filter (Lagoon blue, Lee filters, UK) creating the spectral composition and intensity of irradiance at 45 m depth, while shallow corals were exposed to ambient sunlight. Downwelling irradiance was monitored to ensure that the light levels reflected the ambient conditions in which corals had been collected.

METHOD DETAILS

Biometric measures

To determine microalgal cell density and chlorophyll-*a* content, coral tissue was removed using an airbrush at high pressure with 0.2 µm filtered seawater. Tissue-stripped fragments were bleached in a 6% sodium hypochlorite solution for 24 hours, then rinsed in freshwater for 10 minutes, and left to air dry. The bleached skeletons would be used later in the optical analyses. The microalgae fraction was separated from the host tissue using a motorized homogenizer and centrifugation (5000 rpm for 5 min). Following isolation, samples were immediately stored in a -80ºC freezer for later analyses. Microalgal cell counts were determined using a hemocytometer on five replicate micrographs (scaled 0.1 mm^3). Cell counts were normalized to the coral surface area to quantify areal algal density (cells cm^{-2}). Chlorophyll-*a* was extracted from the remaining algae using 100% cold acetone for 15 h at 4°C and quantified spectrophotometrically [62]. Chlorophyll-*a* was normalized to surface area (µg cm^{-2}) and algae cell (pg $cell^{-1}$). The volume and surface area of the coral subsamples were determined with micro-computed tomography (µCT). The x-ray scans were conducted with a Nikon XT H 225ST µCT (Nikon Metrology Inc., USA) at a resolution of 50-µm voxels. Quantitative analysis was performed using Dragonfly software (v. 2020.1, Object Research Systems (ORS), Inc.).

Chlorophyll-*a* fluorometry

442 The maximum quantum yield of PSII (F_v/F_m) was measured with an imaging pulse-
443 amplitude modulated (PAM) chlorophyll-*a* fluorometer (Maxi-PAM, Walz Gmbh, Germany).
444 Coral samples were dark-acclimated for 20 minutes prior to each measurement (n = 3 per
445 sample). The measured light intensity was adjusted to yield F_0 values in the region of interest
446 that equal about 0.1 [63].
447
448 **O_2 turnover**
449 Photosynthesis-irradiance (*P-E*) curves were performed for individual samples (n = 3-
450 9). Each sample was incubated in a sealed 270 ml acrylic metabolic chamber. The chambers
451 were placed in a temperature-controlled bath (RTE 210, Thermo Neslab), with constant water
452 flow at 22°C (i.e., ambient seawater temperature), and a magnetic stirrer maintaining water
453 movement inside the chamber. A full-spectrum metal halide lamp (400 W, 5000 K, 50 Hz,
454 Golden-Light, Netanya, Israel) was used to incubate the corals at incident downwelling
455 irradiance (E_d) regimes spanning 0 to 800 µmol photons m^{-2} s^{-1}. E_d was measured using a light
456 meter (LI-250A, Li-Cor, Inc. Lincoln, NE, USA) connected to a cosine-corrected quantum
457 sensor. O_2 evolution was monitored within each chamber using O_2 optodes connected to an O_2
458 meter (ProODO Optical Dissolved Oxygen meter, YSI Inc., OH, USA). Areal net
459 photosynthesis (P_n) was calculated from the difference between final and initial O_2
460 measurements (ΔO_2) for each session after 20 minutes under each light intensity. The *P-E* data
461 were fit to a double exponential decay function to characterize the photosynthetic efficiency
462 (α), the maximal photosynthesis rate (P_{MAX}), and the minimum saturation irradiance (E_K) [61].
463 Furthermore, photosynthetic rates were normalized to symbiont cell density and chlorophyll-*a*
464 content to examine the role of the coral host optics in affecting photosynthetic efficiency. Cell-
465 specific gross photosynthetic rates (µmol O_2 $cell^{-1}$ s^{-1}) were based on the assumption that light
466 respiration was up to 1.5-fold higher than dark respiration [50].

467

468 ***Apparent optical properties (AOPs)***

469 Spectral scalar irradiance $E_0(\lambda)$ and diffuse reflectance $R_d(\lambda)$ were measured for intact
470 corals and the bare skeletons of each individual. Measurements were performed in a black
471 acrylic flow chamber. Fiber-optic scalar irradiance microprobes with a tip diameter of 50-100
472 µm (Zenzor, Denmark) were used to measure the surface and intra-tissue light
473 microenvironment as described previously [4]. The microsensors were connected to a
474 spectrometer (AvaSpec-UL2048XL, Avantes, USA) and data were recorded with commercial
475 software (Avasoft 8.0, Avantes, USA). $E_0(\lambda)$ was normalized to the incident downwelling
476 irradiance $E_d(\lambda)$, which was measured under an identical configuration as the experimental
477 coral measurements [4].

478 Spectral reflectance $R_d(\lambda)$ was measured with a flat-cut fiber-optic reflectance probe
479 (diameter = 0.2 cm, Ocean optics, USA) connected to a portable spectrometer (JAZ, Ocean
480 optics, USA). For each measurement, the probe was positioned at 5 mm from the coral/skeleton
481 surface and at a 45° angle relative to the surface [64]. Incident irradiance was provided by a
482 tungsten halogen lamp (Schott ACE 1, Germany) equipped with a collimating lens.
483 Measurements were taken on five randomly chosen areas per coral. Experimental
484 measurements were normalized against a measurement performed on a 99% diffuse reflectance
485 standard (Spectralon, Labsphere USA). Although skeletons were bleached, the reflectance
486 spectrum in the peridinin-chlorophyll-protein complex and chlorophyll-*a* wavebands (490-500
487 and 675 nm, respectively) were slightly affected by pigment residuals (presumably from
488 remaining endolithic algae). Nevertheless, this did not affect the interpretation of the results.

489

490 ***Inherent optical properties (IOPs)***

The transfer of light in corals is described by the radiative transfer equation (RTE). However, the RTE is difficult to solve analytically. In most scattering dominating systems, the RTE can be simplified and expressed as a diffusion dominated process, where optical energy diffuses according to the diffusion equation [65]. Farrell et al. (1992) developed a steady-state diffusion equation for light transport in a semi-infinite planar geometry, where the diffuse reflectance *R* leaving the boundary at a given distance ρ from the source is:

$$R_{(\rho)} = \frac{\alpha'}{4\pi}\left[\frac{1}{\mu_t'}\left(\mu_{eff} + \frac{1}{r_1}\right)\frac{\exp\left(-\mu_{eff} r_1\right)}{{r_1}^2}\right] + \left(\frac{1}{\mu_t'} + \frac{4A}{3\mu_t'}\right) \times \left(\mu_{eff} + \frac{1}{r_2}\right)\frac{\exp\left(-\mu_{eff} r_2\right)}{{r_2}^2} \quad (1)$$

where μ_{eff} is the effective attenuation coefficient:

$$\mu_{eff} = 3\mu_a\sqrt{(\mu_a + \mu_s')} \quad (1.1)$$

a' is the transport albedo:

$$a' = \frac{\mu_s'}{(\mu_a + \mu_s')} \quad (1.2)$$

μ_t is the total interaction coefficient:

$$\mu_t = \mu_a + \mu_s' \quad (1.3)$$

And r_1 and r_2 are radial distances of one mean free path inside the medium and above the medium where total fluence equals 0, respectively [66]. The optical properties μ_s' and μ_a uniquely determine the shape of the diffuse reflectance curve. By measuring the lateral spread (*r*) of reflected light (*R*) it is thus possible to predict unique values of μ_s' and the absorption coefficient μ_a that generated the reflectance profile. The fitting procedure uses the fminsearch.m routine in Matlab (Mathworks, USA) which calls a multidimensional unconstrained non-linear minimization algorithm (Nelder–Mead) to minimize the sum of

515 squares error [41,67]. Optical extraction of μ_s' and μ_a were performed for intact corals at
516 wavelengths of strong chlorophyll-*a* absorption (at 663 nm) as well as in the near-infrared (at
517 750nm), which is free from pigment absorption.

518 We extracted scattering (μ_s') and absorption (μ_a) coefficients [68] from intact corals
519 and skeletons by measuring the lateral spread of reflected light (R_r). Measurements were
520 performed with a flat cut light-emitting source fiber (diameter = 0.2 cm, Ocean optics, USA)
521 connected to a tungsten halogen lamp (LS-1, Ocean Optics, USA) and a flat-cut light collecting
522 fiber (diameter = 50 µm, Zenzor, Denmark) connected to a spectrometer (AvaSpec-
523 UL2048XL, Avantes, USA). Both fibers were mounted on micromanipulators (Pyroscience
524 GmBH, Germany and Märtzhäuser, Germany) and aligned parallel to each other at a minimum
525 lateral distance of 4 mm perpendicular to and in direct contact with the coral surface. A
526 stereomicroscope (SZ51, Olympus) was used to carefully position the fiber optic probes at the
527 surface. R_r was measured at lateral steps of 1 mm to a maximum of 10 mm [67]. This procedure
528 was repeated for five randomly chosen coenosarc areas for each coral sample. Measurements
529 were conducted on the coenosarc, which had a more even topography and less contractile tissue
530 compared with the polyp tissue, thus allowing repeated measurements and a more accurate
531 estimate of horizontal light transfer. The lateral attenuation of light was matched to the
532 predicted attenuation pR_r based on diffusion theory [66] and starting values of μ_s', μ_a. The coral
533 surface architecture for *P. peresi* was very heterogeneous due to the deep corallite architecture,
534 preventing reliable quantification of *R(r)*, and the analysis was thus omitted.

535 Additionally, we characterized the algal cell-specific absorption coefficient (μ_{a_algae})
536 of isolated symbionts independent of the host environment. To separate between the effect of
537 algal absorption and that of algal scattering, diffuse reflectance measurements were performed
538 in a strongly scattering dominated medium, such that any algal scattering can be regarded as
539 negligible. Milk is a cost-effective strongly scattering-medium with known optical properties.

The lipid content of 100% whole milk is typically 4% lipids and the scattering of intralipid^{TM} in 10% lipids is 100 cm^{-1} (at 600 nm). Therefore, the scattering of 100% whole milk is estimated to be:

$$\mu_s'(\lambda)_{milk} = (40\ cm^{-1})(\frac{\lambda}{600nm})^{-1} \qquad (2)$$

Reflectance measurements were performed with 100% whole milk and a 1:1 mixture of milk and algal serial dilutions (from 50% to 3%). Algal cell density was determined as described above in order to relate μ_{a_algae} to cell density (mL^{-1}). To extract μ_{a_algae} [cm^{-1}] diffusion theory and nonlinear least-squares fitting were used as described above to match predicted reflectance to experimentally measured reflectance.

Monte Carlo modeling of absorbed flux

To characterize differences in light absorption by coral tissues we developed a Monte Carlo simulation using the inherent optical properties determined via diffusion theory as input parameters (Fig. 6, Table 1). For each simulation the tissue was 1mm thick and had an absorption coefficient μ_a that was determined by μ_a algae at 675 nm. Tissue μ_s' was set to 5 cm^{-1} for all simulations. Details on the Monte Carlo approach can be found in Wangpraseurt et al. [41] and Jacques et al [67].

QUANTIFICATION AND STATISTICAL ANALYSIS

All statistical analyses were performed using the R software (R Core Team 2020). To estimate ecophysiological and bio-optical variations in the studied species, we modeled the corresponding parameters (separate test for each parameter) as a function of species and depth, using mixed-effects permutational analysis (MEPA; 2000 permutations), with coral identity as a random effect. These analyses were run using the packages {nlme}[70] and

564 {predictmeans}[71]. Pairwise comparisons were based on Hedge's *g* (*Hg*) standardized effect
565 size (preferred over Cohen's *d* for small samples) with 95% confidence interval (CI)
566 constructed from 5000 bootstrap samples, and significance was determined as CI not
567 overlapping with zero (shallow depth as reference). This analysis was computed using the R
568 package {dabestr}[72].
569

570 ## References

571 1. Graham, N.A.J., and Nash, K.L. (2013). The importance of structural complexity in
572 coral reef ecosystems. Coral Reefs.
573 2. Roth, M.S. (2014). The engine of the reef: Photobiology of the coral-algal symbiosis.
574 Front. Microbiol. *5*, 1–22.
575 3. Enríquez, S., Méndez, E.R., and Iglesias-Prieto, R. (2005). Multiple scattering on coral
576 skeletons enhances light absorption by symbiotic algae. Limnol. Oceanogr. *50*, 1025–
577 1032.
578 4. Wangpraseurt, D., Larkum, A.W.D., Ralph, P.J., and Kühl, M. (2012). Light gradients
579 and optical microniches in coral tissues. Front. Microbiol. *3*, 1–9.
580 5. Kahng, S.E., Hochberg, E.J., Apprill, A., Wagner, D., Luck, D.G., Perez, D., and
581 Bidigare, R.R. (2012). Efficient light harvesting in deep-water zooxanthellate corals.
582 Mar. Ecol. Prog. Ser. *455*, 65–77.
583 6. Brodersen, K.E., Lichtenberg, M., Ralph, P.J., Kühl, M., and Wangpraseurt, D. (2014).
584 Radiative energy budget reveals high photosynthetic efficiency in symbiont-bearing
585 corals. J. R. Soc. Interface *11*, 20130997.
586 7. Hughes, T.P., Kerry, J.T., Baird, A.H., Connolly, S.R., Dietzel, A., Eakin, C.M.,
587 Heron, S.F., Hoey, A.S., Hoogenboom, M.O., Liu, G., *et al.* (2018). Global warming
588 transforms coral reef assemblages.

589 8. Baker, A.C., Glynn, P.W., and Riegl, B. (2008). Climate change and coral reef
590 bleaching: An ecological assessment of long-term impacts, recovery trends and future
591 outlook. Estuar. Coast. Shelf Sci. *80*, 435–471. Available at:
592 http://linkinghub.elsevier.com/retrieve/pii/S0272771408003405 [Accessed March 23,
593 2017].
594 9. Leggat, W.P., Camp, E.F., Suggett, D.J., Heron, S.F., Fordyce, A.J., Gardner, S.,
595 Deakin, L., Turner, M., Beeching, L.J., Kuzhiumparambil, U., *et al.* (2019). Rapid
596 Coral Decay Is Associated with Marine Heatwave Mortality Events on Reefs. Curr.
597 Biol., 1–8. Available at:
598 https://linkinghub.elsevier.com/retrieve/pii/S0960982219308048.
599 10. Ward, S., Harrison, P., and Hoegh-Guldberg, O. (2000). Coral bleaching reduces
600 reproduction of scleractinian corals and increases susceptibility to future stress. Proc.
601 9th Int. Coral Reef Symp. *2*.
602 11. Hughes, T.P., Kerry, J.T., Baird, A.H., Connolly, S.R., Chase, T.J., Dietzel, A., Hill,
603 T., Hoey, A.S., Hoogenboom, M.O., Jacobson, M., *et al.* (2019). Global warming
604 impairs stock–recruitment dynamics of corals. Nature. Available at:
605 https://doi.org/10.1038/s41586-019-1081-y.
606 12. Shlesinger, T., and Loya, Y. (2019). Breakdown in spawning synchrony: A silent
607 threat to coral persistence. Science (80-.). *365*, 1002 LP – 1007. Available at:
608 http://science.sciencemag.org/content/365/6457/1002.abstract.
609 13. Bruno, J.F., Selig, E.R., Casey, K.S., Page, C.A., Willis, B.L., Harvell, C.D.,
610 Sweatman, H., and Melendy, A.M. (2007). Thermal Stress and Coral Cover as Drivers
611 of Coral Disease Outbreaks. PLOS Biol. *5*, e124. Available at:
612 https://doi.org/10.1371/journal.pbio.0050124.
613 14. Ortiz, J.-C., Wolff, N.H., Anthony, K.R.N., Devlin, M., Lewis, S., and Mumby, P.J.

(2018). Impaired recovery of the Great Barrier Reef under cumulative stress. Sci. Adv. *4*, eaar6127. Available at: http://advances.sciencemag.org/content/4/7/eaar6127.abstract.

15. Hughes, T.P., Kerry, J.T., Álvarez-Noriega, M., Álvarez-Romero, J.G., Anderson, K.D., Baird, A.H., Babcock, R.C., Beger, M., Bellwood, D.R., Berkelmans, R., *et al.* (2017). Global warming and recurrent mass bleaching of corals. Nature *543*, 373–377. Available at: http://dx.doi.org/10.1038/nature21707.

16. Richmond, R.H., Tisthammer, K.H., and Spies, N.P. (2018). The Effects of Anthropogenic Stressors on Reproduction and Recruitment of Corals and Reef Organisms. Front. Mar. Sci. *5*. Available at: https://www.frontiersin.org/article/10.3389/fmars.2018.00226/full.

17. Boström-Einarsson, L., Babcock, R.C., Bayraktarov, E., Ceccarelli, D., Cook, N., Ferse, S.C.A., Hancock, B., Harrison, P., Hein, M., Shaver, E., *et al.* (2020). Coral restoration – A systematic review of current methods, successes, failures and future directions. PLoS One *15*, e0226631. Available at: https://doi.org/10.1371/journal.pone.0226631.

18. Bongaerts, P., Ridgway, T., Sampayo, E.M., and Hoegh-Guldberg, O. (2010). Assessing the "deep reef refugia" hypothesis: Focus on Caribbean reefs. Coral Reefs *29*, 1–19. Available at: http://dx.doi.org/10.1007/s00338-009-0581-x.

19. Glynn, P.W. (1996). Coral reef bleaching: Facts, hypotheses and implications. Glob. Chang. Biol.

20. Loya, Y., Eyal, G., Treibitz, T., Lesser, M.P., and Appeldoorn, R. (2016). Theme section on mesophotic coral ecosystems: advances in knowledge and future perspectives. Coral Reefs *35*, 1–9.

21. Rocha, L.A., Pinheiro, H.T., Shepherd, B., Papastamatiou, Y.P., Luiz, O.J., Pyle, R.L.,

and Bongaerts, P. (2018). Mesophotic coral ecosystems are threatened and ecologically distinct from shallow water reefs. Science (80-.). *361*, 281–284. Available at: http://www.sciencemag.org/lookup/doi/10.1126/science.aaq1614.

22. Pinheiro, H.T., Eyal, G., Shepherd, B., and Rocha, L.A. (2019). Ecological insights from environmental disturbances in mesophotic coral ecosystems. Ecosphere *10*, e02666. Available at: https://onlinelibrary.wiley.com/doi/abs/10.1002/ecs2.2666.

23. Frade, P.R., Bongaerts, P., Englebert, N., Rogers, A., Gonzalez-Rivero, M., and Hoegh-Guldberg, O. (2018). Deep reefs of the Great Barrier Reef offer limited thermal refuge during mass coral bleaching. Nat. Commun. *9*, 3447. Available at: http://www.nature.com/articles/s41467-018-05741-0.

24. Grottoli, A.G., Warner, M.E., Levas, S.J., Aschaffenburg, M.D., Schoepf, V., Mcginley, M., Baumann, J., and Matsui, Y. (2014). The cumulative impact of annual coral bleaching can turn some coral species winners into losers. Glob. Chang. Biol. *20*, 3823–3833.

25. Smith, L.W., Barshis, D., and Birkeland, C. (2007). Phenotypic plasticity for skeletal growth, density and calcification of Porites lobata in response to habitat type. Coral Reefs *26*, 559–567.

26. Doszpot, N., McWilliam, M., Pratchett, M., Hoey, A., and Figueira, W. (2019). Plasticity in Three-Dimensional Geometry of Branching Corals Along a Cross-Shelf Gradient. Diversity *11*, 44. Available at: https://www.mdpi.com/1424-2818/11/3/44.

27. Kahng, S.E., Akkaynak, D., Shlesinger, T., Hochberg, E.J., Wiedenmann, J., Tamir, R., and Tchernov, D. (2019). Light, Temperature, Photosynthesis, Heterotrophy, and the Lower Depth Limits of Mesophotic Coral Ecosystems. In Mesophotic Coral Ecosystems, Y. Loya, K. A. Puglise, and T. C. L. Bridge, eds. (Cham: Springer International Publishing), pp. 801–828. Available at: https://doi.org/10.1007/978-3-

319-92735-0_42.

28. Pratchett, M.S., Anderson, K.D., Hoogenboom, M.O., Widman, E., Baird, A.H., Pandolfi, J.M., Edmunds, P.J., and Lough, J.M. (2015). Spatial, Temporal and Taxonomic Variation in Coral Growth–Implications for the Strucutre and Function of Coral Reef Ecosystems. Oceanogr. Mar. Biol. An Annu. Rev. *53*, 215–296.

29. Kramer, N., Tamir, R., Eyal, G., and Loya, Y. (2020). Coral Morphology Portrays the Spatial Distribution and Population Size-Structure Along a 5–100 m Depth Gradient. Front. Mar. Sci. *7*, 615. Available at: https://www.frontiersin.org/article/10.3389/fmars.2020.00615.

30. Tamir, R., Eyal, G., Kramer, N., Laverick, J.H., and Loya, Y. (2019). Light environment drives the shallow to mesophotic coral community transition. Ecosphere *10*, e02839.

31. Semmler, R.F., Hoot, W.C., and Reaka, M.L. (2016). Are mesophotic coral ecosystems distinct communities and can they serve as refugia for shallow reefs? Coral Reefs. Available at: http://link.springer.com/10.1007/s00338-016-1530-0.

32. Kramer, N., Eyal, G., Tamir, R., and Loya, Y. (2019). Upper mesophotic depths in the coral reefs of Eilat, Red Sea, offer suitable refuge grounds for coral settlement. Sci. Rep. *9*, 2263. Available at: http://www.nature.com/articles/s41598-019-38795-1.

33. Turner, J.A., Thomson, D.P., Cresswell, A.K., Trapon, M., Babcock, R.C., and Turner, J.A. (2018). Depth-related patterns in coral recruitment across a shallow to mesophotic gradient. Coral Reefs. Available at: https://doi.org/10.1007/s00338-018-1696-8.

34. Goodbody-Gringley, G., Wong, K.H., Becker, D.M., Glennon, K., and de Putron, S.J. (2018). Reproductive ecology and early life history traits of the brooding coral, Porites astreoides, from shallow to mesophotic zones. Coral Reefs. Available at: https://doi.org/10.1007/s00338-018-1673-2.

689 35. Shlesinger, T., and Loya, Y. (2019). Sexual Reproduction of Scleractinian Corals in
690 Mesophotic Coral Ecosystems vs. Shallow Reefs. In Mesophotic Coral Ecosystems, Y.
691 Loya, K. A. Puglise, and T. C. L. Bridge, eds. (Cham: Springer International
692 Publishing), pp. 653–666. Available at: https://doi.org/10.1007/978-3-319-92735-
693 0_35.
694 36. Studivan, M.S., Milstein, G., and Voss, J.D. (2019). Montastraea cavernosa corallite
695 structure demonstrates distinct morphotypes across shallow and mesophotic depth
696 zones in the Gulf of Mexico. PLoS One *14*.
697 37. Anthony, K.R.N., Hoogenboom, M.O., and Connolly, S.R. (2005). Adaptive variation
698 in coral geometry and the optimization of internal colony light climates. Funct. Ecol.
699 *19*, 17–26. Available at:
700 https://besjournals.onlinelibrary.wiley.com/doi/abs/10.1111/j.0269-
701 8463.2005.00925.x.
702 38. Winters, G., Beer, S., Ben Zvi, B., Brickner, I., and Loya, Y. (2009). Spatial and
703 temporal photoacclimation of stylophora pistillata: Zooxanthella size, pigmentation,
704 location and clade. Mar. Ecol. Prog. Ser. *384*, 107–119.
705 39. McCloskey, L.R., and Muscatine, L. (1984). Production and respiration in the Red Sea
706 coral Stylophora pistillata as a function of depth. Proc. R. Soc. B Biol. Sci.
707 40. Wangpraseurt, D., Jacques, S., Lyndby, N., Holm, J.B., Pages, C.F., and Kühl, M.
708 (2019). Microscale light management and inherent optical properties of intact corals
709 studied with optical coherence tomography. J. R. Soc. Interface *16*.
710 41. Wangpraseurt, D., Jacques, S.L., Petrie, T., and Kühl, M. (2016). Monte Carlo
711 Modeling of Photon Propagation Reveals Highly Scattering Coral Tissue. Front. Plant
712 Sci. *7*, 1–10. Available at:
713 http://journal.frontiersin.org/Article/10.3389/fpls.2016.01404/abstract.

714 42. Swain, T.D., DuBois, E., Gomes, A., Stoyneva, V.P., Radosevich, A.J., Henss, J.,
715 Wagner, M.E., Derbas, J., Grooms, H.W., Velazquez, E.M., *et al.* (2016). Skeletal
716 light-scattering accelerates bleaching response in reef-building corals (BioMed
717 Central).
718 43. Eyal, G., Wiedenmann, J., Grinblat, M., D'Angelo, C., Kramarsky-Winter, E.,
719 Treibitz, T., Ben-Zvi, O., Shaked, Y., Smith, T.B., Harii, S., *et al.* (2015). Spectral
720 diversity and regulation of coral fluorescence in a mesophotic reef habitat in the Red
721 Sea. PLoS One.
722 44. Einbinder, S., Gruber, D.F., Salomon, E., Liran, O., Keren, N., and Tchernov, D.
723 (2016). Novel Adaptive Photosynthetic Characteristics of Mesophotic Symbiotic
724 Microalgae within the Reef-Building Coral, Stylophora pistillata. Front. Mar. Sci. *3*,
725 195.
726 45. Kahng, S.E., Watanabe, T.K., Hu, H.-M., Watanabe, T., and Shen, C.-C. (2020).
727 Moderate zooxanthellate coral growth rates in the lower photic zone. Coral Reefs.
728 Available at: https://doi.org/10.1007/s00338-020-01960-4.
729 46. Fricke, H., and Meischner, D. (1985). Depth limits of Bermudan scleractinian corals: a
730 submersible survey. Mar. Biol. *88*, 175–187.
731 47. Smith, E.G., D'Angelo, C., Sharon, Y., Tchernov, D., and Wiedenmann, J. (2017).
732 Acclimatization of symbiotic corals to mesophotic light environments through
733 wavelength transformation by fluorescent protein pigments. Proc. R. Soc. B Biol. Sci.
734 48. Turner, J.A., Andradi-Brown, D.A., Gori, A., Bongaerts, P., Burdett, H.L., Ferrier-
735 Pagès, C., Voolstra, C.R., Weinstein, D.K., Bridge, T.C.L., Costantini, F., *et al.*
736 (2019). Key Questions for Research and Conservation of Mesophotic Coral
737 Ecosystems and Temperate Mesophotic Ecosystems. In Mesophotic Coral Ecosystems,
738 Y. Loya, K. A. Puglise, and T. C. L. Bridge, eds. (Cham: Springer International

739 Publishing), pp. 989–1003. Available at: https://doi.org/10.1007/978-3-319-92735-
740 0_52.
741 49. Mass, T., Einbinder, S., Brokovich, E., Shashar, N., Vago, R., Erez, J., and Dubinsky,
742 Z. (2007). Photoacclimation of Stylophora pistillata to light extremes: Metabolism and
743 calcification. Mar. Ecol. Prog. Ser. *334*, 93–102.
744 50. Wangpraseurt, D., Holm, J.B., Larkum, A.W.D., Pernice, M., Ralph, P.J., Suggett,
745 D.J., and Kühl, M. (2017). In vivo microscale measurements of light and
746 photosynthesis during coral bleaching: Evidence for the optical feedback loop? Front.
747 Microbiol. *8*, 1–12.
748 51. Veron, C., Stafford-Smith, M., Turak, E., and DeVantier, L. (2000). Corals of the
749 world.
750 52. Houlbrèque, F., and Ferrier-Pagès, C. (2009). Heterotrophy in tropical scleractinian
751 corals. Biol. Rev. *84*, 1–17.
752 53. Falkowski, P.G., and Dubinsky, Z. (1981). Light-shade adaptation of Stylophora
753 pistillata, a hermatypic coral from the Gulf of Eilat. Nature *289*, 172–174.
754 54. Marcelino, L.A., Westneat, M.W., Stoyneva, V., Henss, J., Rogers, J.D., Radosevich,
755 A., Turzhitsky, V., Siple, M., Fang, A., Swain, T.D., *et al.* (2013). Modulation of
756 Light-Enhancement to Symbiotic Algae by Light-Scattering in Corals and
757 Evolutionary Trends in Bleaching. PLoS One.
758 55. Malik, A., Einbinder, S., Martinez, S., Tchernov, D., Haviv, S., Almuly, R., Zaslansky,
759 P., Polishchuk, I., Pokroy, B., Stolarski, J., *et al.* (2020). Molecular and skeletal
760 fingerprints of scleractinian coral biomineralization: From the sea surface to
761 mesophotic depths. Acta Biomater., 1–14. Available at:
762 https://doi.org/10.1016/j.actbio.2020.01.010.
763 56. Cunning, R., and Baker, A.C. (2013). Excess algal symbionts increase the

susceptibility of reef corals to bleaching. Nat. Clim. Chang. *3*, 259–262. Available at: https://doi.org/10.1038/nclimate1711.

57. Fantazzini, P., Mengoli, S., Pasquini, L., Bortolotti, V., Brizi, L., Mariani, M., Di Giosia, M., Fermani, S., Capaccioni, B., Caroselli, E., *et al.* (2015). Gains and losses of coral skeletal porosity changes with ocean acidification acclimation. Nat. Commun. *6*.

58. Mollica, N.R., Guo, W., Cohen, A.L., Huang, K.-F., Foster, G.L., Donald, H.K., and Solow, A.R. (2018). Ocean acidification affects coral growth by reducing skeletal density. Proc. Natl. Acad. Sci. *115*, 1754–1759. Available at: http://www.pnas.org/lookup/doi/10.1073/pnas.1712806115.

59. Foster, T., Falter, J.L., McCulloch, M.T., and Clode, P.L. (2016). Ocean acidification causes structural deformities in juvenile coral skeletons. Sci. Adv. *2*, 1–8.

60. Teixidó, N., Gambi, M.C., Parravacini, V., Kroeker, K., Micheli, F., Villéger, S., and Ballesteros, E. (2018). Functional biodiversity loss along natural CO2 gradients. Nat. Commun. *9*, 1–9. Available at: http://dx.doi.org/10.1038/s41467-018-07592-1.

61. Platt, T., Gallegos, C.L., and Harrison, W.G. (1980). Photoinhibition of photosynthesis in natural assemblages of marine phytoplankton. J. Mar. Res. *38*, 687–701. Available at: https://www.scopus.com/inward/record.uri?eid=2-s2.0-0019089393&partnerID=40&md5=8a1c3c6fd1208c2f3ebb6dc553f9795f.

62. Jeffrey, S.W., and Humphrey, G.F. (1975). New spectrophotometric equations for determining chlorophylls a, b, c1 and c2 in higher plants, algae and natural phytoplankton. Biochem. und Physiol. der Pflanz.

63. Wangpraseurt, D., Lichtenberg, M., Jacques, S.L., Larkum, A.W.D., and Kühl, M. (2019). Optical Properties of Corals Distort Variable Chlorophyll Fluorescence Measurements. Plant Physiol. *179*, 1608–1619.

64. Wangpraseurt, D., Wentzel, C., Jacques, S.L., Wagner, M., and Kühl, M. (2017). In

vivo imaging of coral tissue and skeleton with optical coherence tomography. J. R. Soc. Interface *14*.

65. Jacques, S.L., and Pogue, B.W. (2008). Tutorial on diffuse light transport. J. Biomed. Opt. *13*, 041302.

66. Farrell, T.J., Patterson, M.S., and Wilson, B. (1992). A diffusion theory model of spatially resolved, steady-state diffuse reflectance for the noninvasive determination of tissue optical properties in vivo. Med. Phys. *19*, 879–888.

67. Jacques, S.L., Wangpraseurt, D., and Kühl, M. (2019). Optical Properties of Living Corals Determined With Diffuse Reflectance Spectroscopy. Front. Mar. Sci. *6*, 1–9.

68. Jacques, S.L. (2013). Optical properties of biological tissues: a review. Phys. Med. Biol. *58*, R37--R61. Available at: https://doi.org/10.1088%2F0031-9155%2F58%2F11%2Fr37.

69. Team, R.C. (2020). R: A Language and Environment for Statistical Computing. R Foundation for Statistical Computing, Vienna, Austria. URL https://www.R-project.org/.

70. Pinheiro, J., Bates, D., DebRoy, S., Sarkar, D., and Team, R.C. (2020). {nlme}: Linear and Nonlinear Mixed Effects Model. Available at: http://cran.r-project.org/package=nlme.

71. Luo, D., Ganesh, S., and Koolaard, J. (2020). predictmeans: Calculate Predicted Means for Linear Models. Available at: http://cran.r-project.org/package=predictmeans.

72. Ho, J., Tumkaya, T., Aryal, S., Choi, H., and Claridge-Chang, A. (2019). Moving beyond P values: data analysis with estimation graphics. Nat. Methods *16*, 565–566. Available at: https://doi.org/10.1038/s41592-019-0470-3.

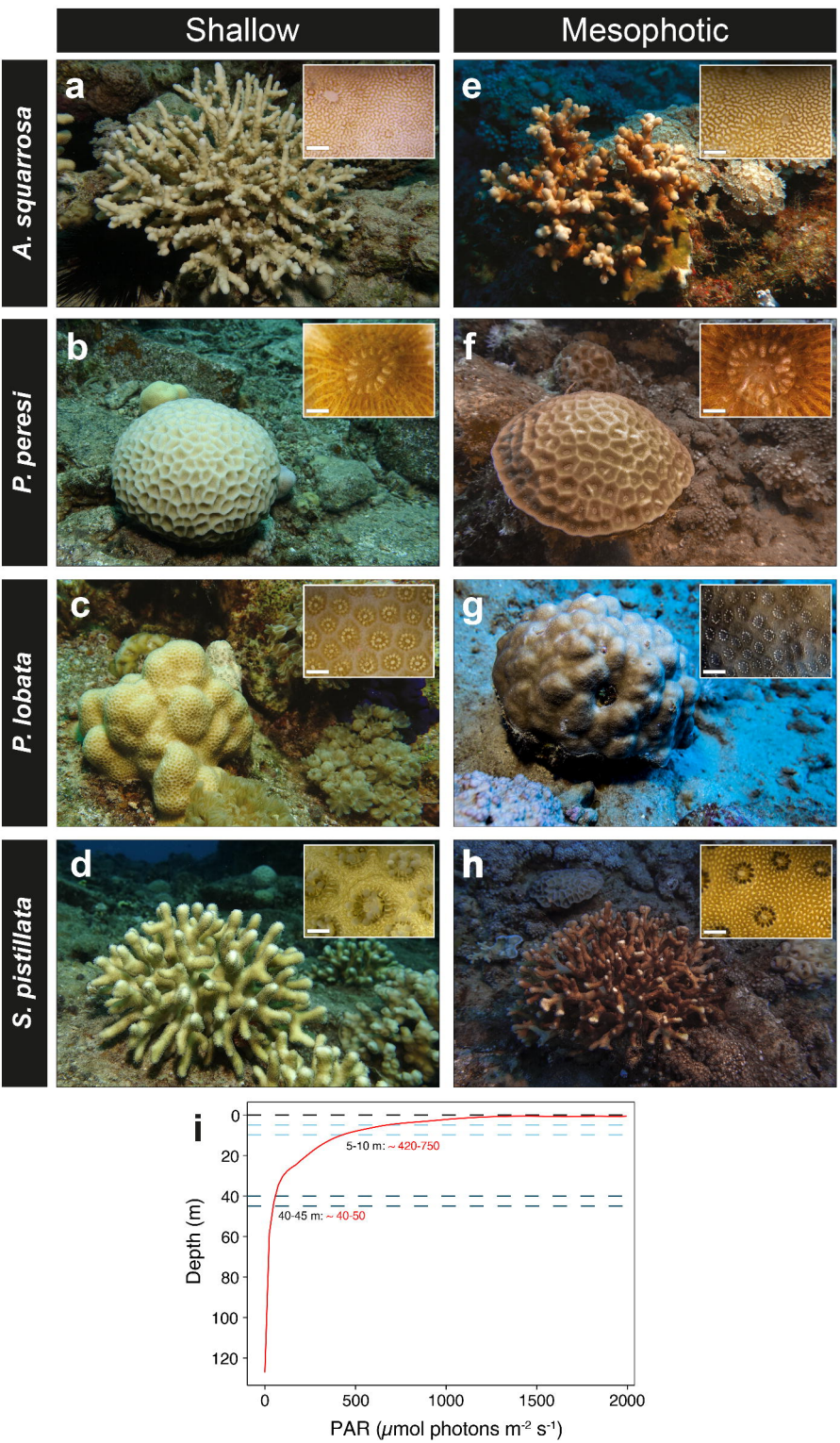
Shallow
Mesophotic
A. squarrosa
P. peresi
P. lobata
S. pistillata
a
b
c
d
e
f
g
h
i
Depth (m)
0
20
40
60
80
100
120
5-10 m: ~ 420-750
40-45 m: ~ 40-50
0
500
1000
1500
2000
PAR (μmol photons m-2 s-1)

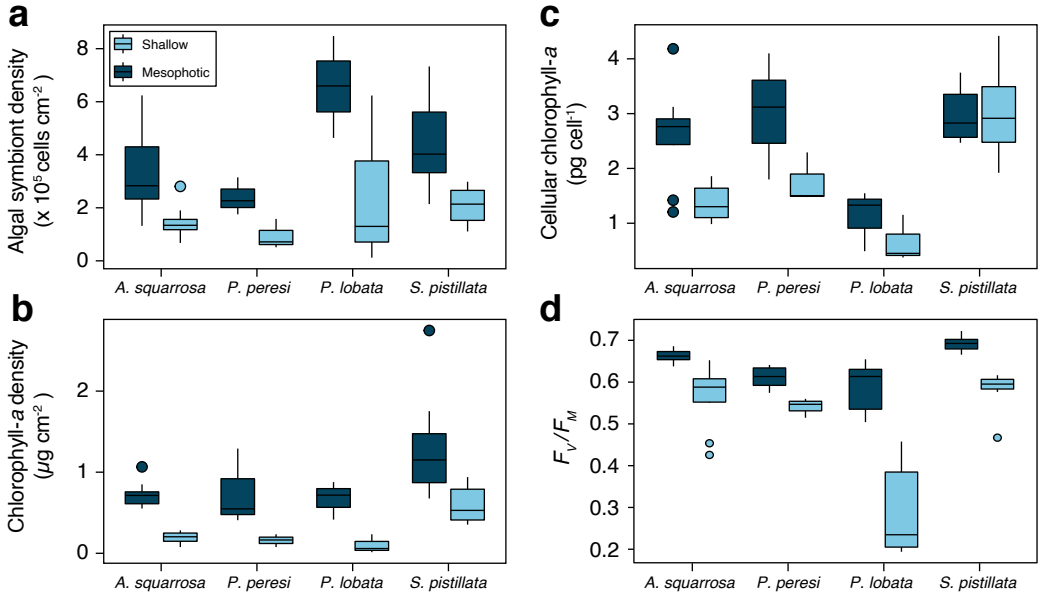
a
Shallow
Mesophotic
Algal symbiont density
(x 10^5 cells cm^-2)
0
2
4
6
8
A. squarrosa
P. peresi
P. lobata
S. pistillata
b
Chlorophyll-a density
(μg cm^-2)
0
1
2
A. squarrosa
P. peresi
P. lobata
S. pistillata
c
Cellular chlorophyll-a
(pg cell^-1)
1
2
3
4
A. squarrosa
P. peresi
P. lobata
S. pistillata
d
F_V/F_M
0.2
0.3
0.4
0.5
0.6
0.7
A. squarrosa
P. peresi
P. lobata
S. pistillata

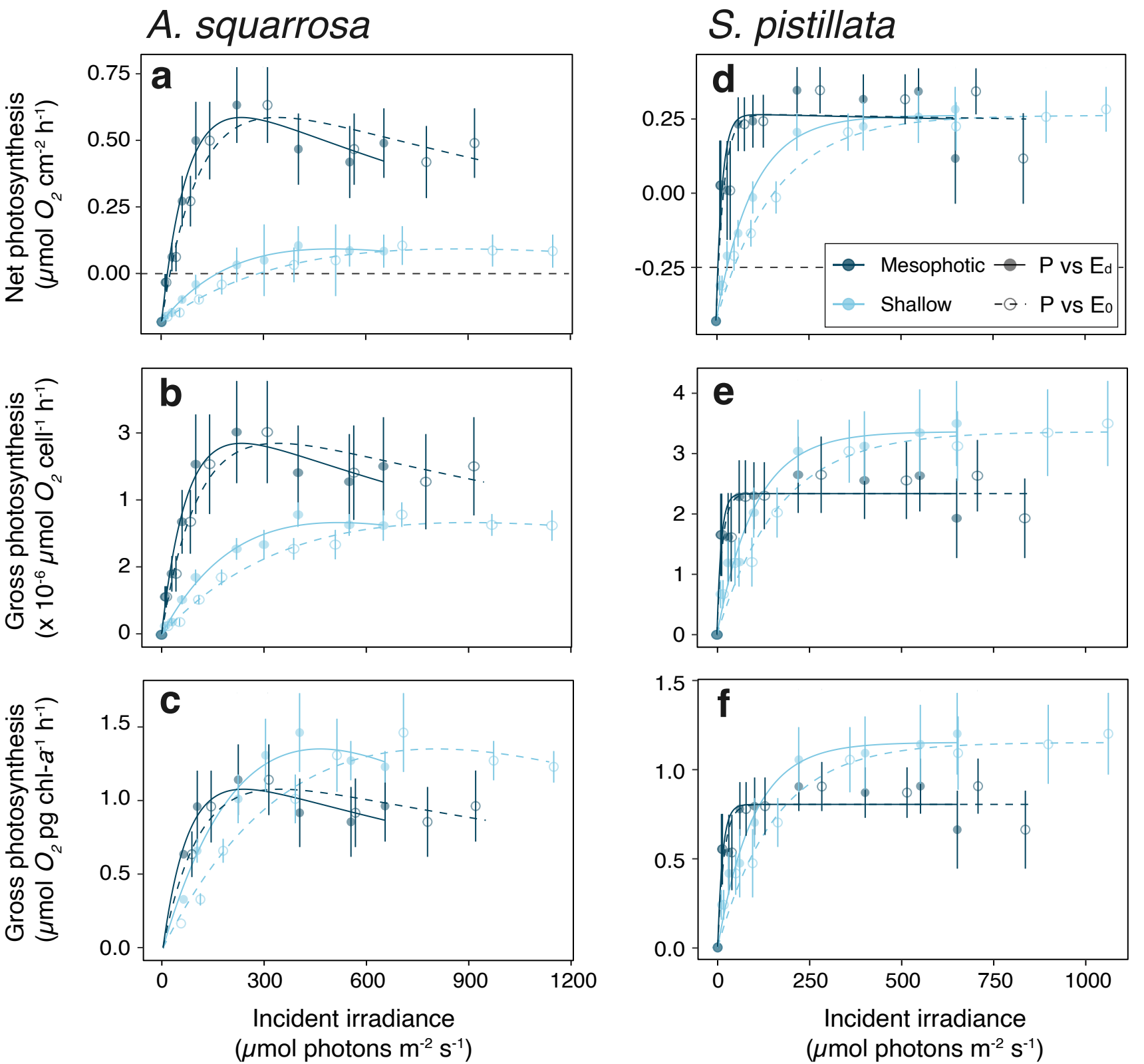
A. squarrosa
S. pistillata
a
b
c
d
e
f
Net photosynthesis (μmol O2 cm-2 h-1)
Gross photosynthesis (x 10-6 μmol O2 cell-1 h-1)
Gross photosynthesis (μmol O2 pg chl-a-1 h-1)
Mesophotic
Shallow
P vs Ed
P vs E0
Incident irradiance (μmol photons m-2 s-1)
Incident irradiance (μmol photons m-2 s-1)

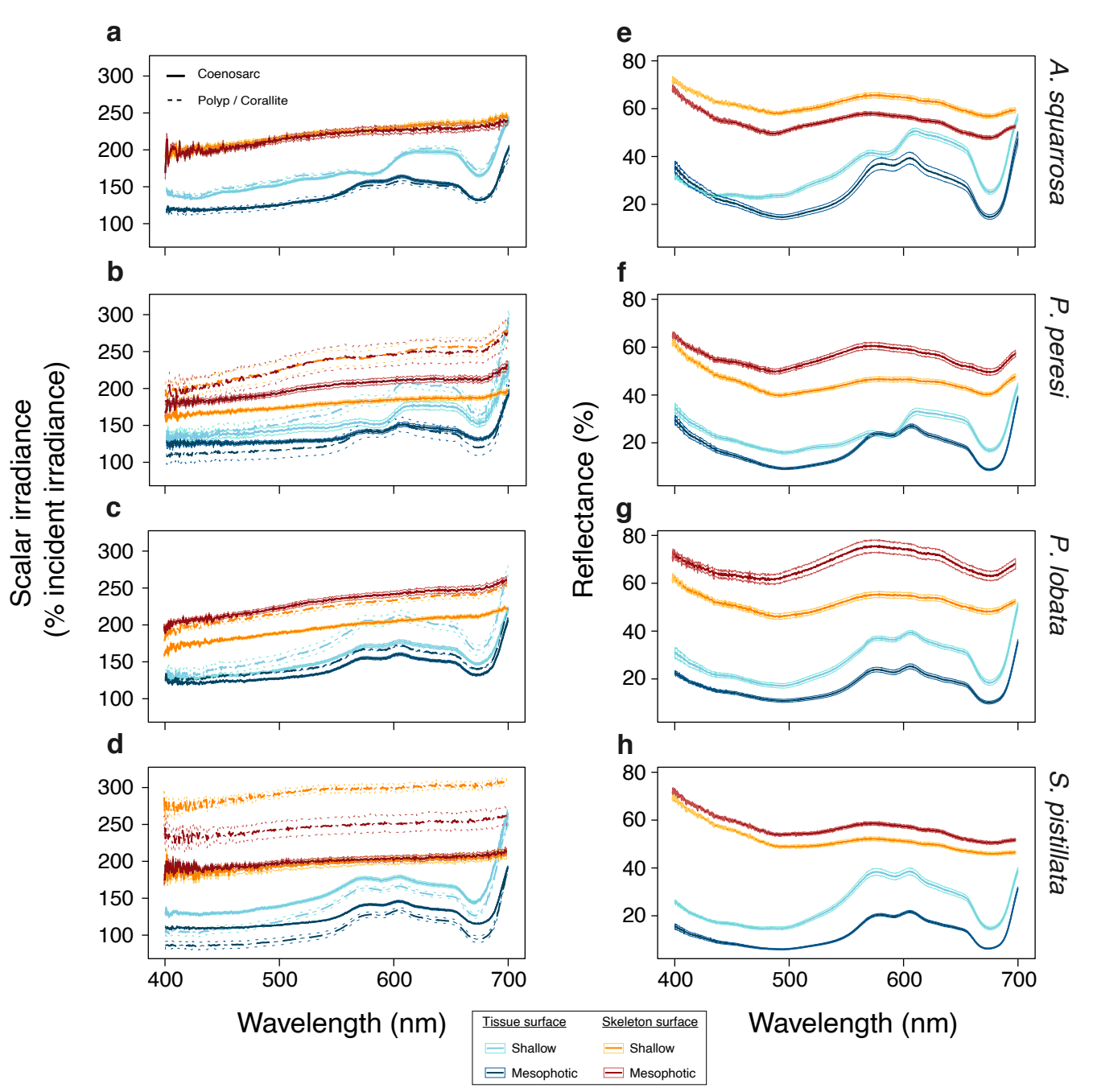
a
b
c
d
e
f
g
h
Coenosarc
Polyp / Corallite
Scalar irradiance
(% incident irradiance)
Reflectance (%)
Wavelength (nm)
Wavelength (nm)
A. squarrosa
P. peresi
P. lobata
S. pistillata
Tissue surface
Shallow
Mesophotic
Skeleton surface
Shallow
Mesophotic